Electronic Supplementary Information (ESI)

Metastable marcasite $NiSe_2$ nanodendrites on carbon fiber clothes to suppress polysulfide shuttling for high-performance lithium-sulfur batteries

Jingwen Wang,[a] Shoufu Cao,[b] Likun Yang,[a] Yan Zhang,[a] Kun Xing,*[a] Xiaoqing Lu,*[b] and Jun Xu*[a]

[a]School of Microelectronics, Hefei University of Technology, Hefei 230009, P.R. China. E-mail: k.xing@hfut.edu.cn (K. Xing), apjunxu@hfut.edu.cn (J. Xu)

[b]School of Materials Science and Engineering, China University of Petroleum (East China), Qingdao 266580, P.R. China. E-mail: luxq@upc.edu.cn (X. Lu)

Table S1 The parameters of the assembled LSBs.

Cell configuration	Sulfur mass (mg)	Areal sulfur loading (mg cm^{-2})	Electrolyte amount (μL)	E/S ratio (μL mg^{-1})	Sulfur/Carbon (CFC+rGO) ratio
Al@S/rGO@m-$NiSe_2$/CFC	1.24	1.1	30	24.2	0.076
Al@S/rGO@p-$NiSe_2$/CFC	1.24	1.1	30	24.2	0.076
m-$NiSe_2$/CFC@S/rGO@CFC	2.26	2.0	40	17.7	0.069
p-$NiSe_2$/CFC@S/rGO@CFC	2.26	2.0	40	17.7	0.069
m-$NiSe_2$/CFC@S/ rGO @m-$NiSe_2$/CFC	5.09	4.5	45	8.8	0.153
	2.83	2.5	40	16	0.087
p-$NiSe_2$/CFC@S/ rGO@p-$NiSe_2$/CFC	2.83	2.5	40	16	0.087

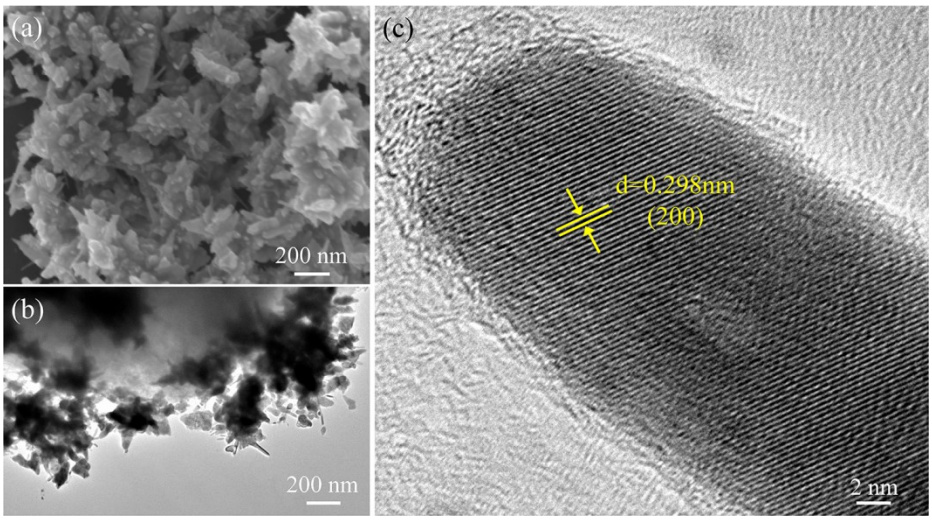

Fig. S1 SEM, TEM, and HRTEM images of the p-$NiSe_2$/CFC sample.

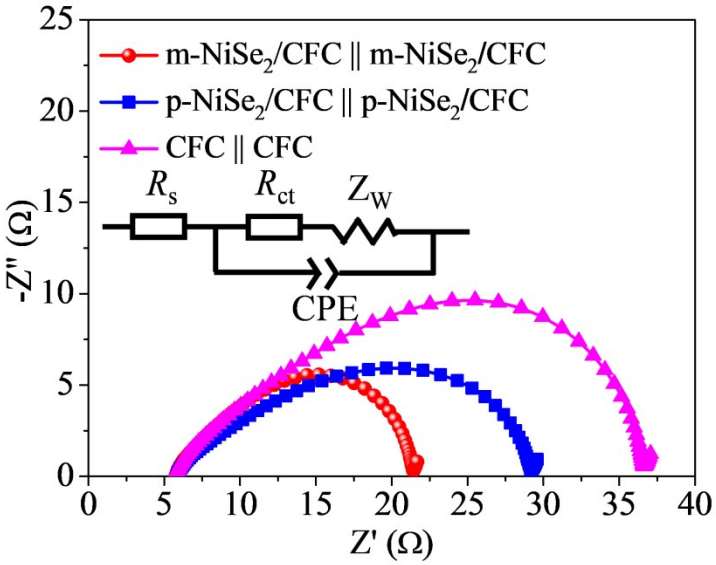

Fig. S2 Nyquist plots of the symmetric cells of m-$NiSe_2$/CFC||m-$NiSe_2$/CFC, p-$NiSe_2$/CFC||p-$NiSe_2$/CFC and CFC||CFC, inset is the corresponding equivalent circuit.

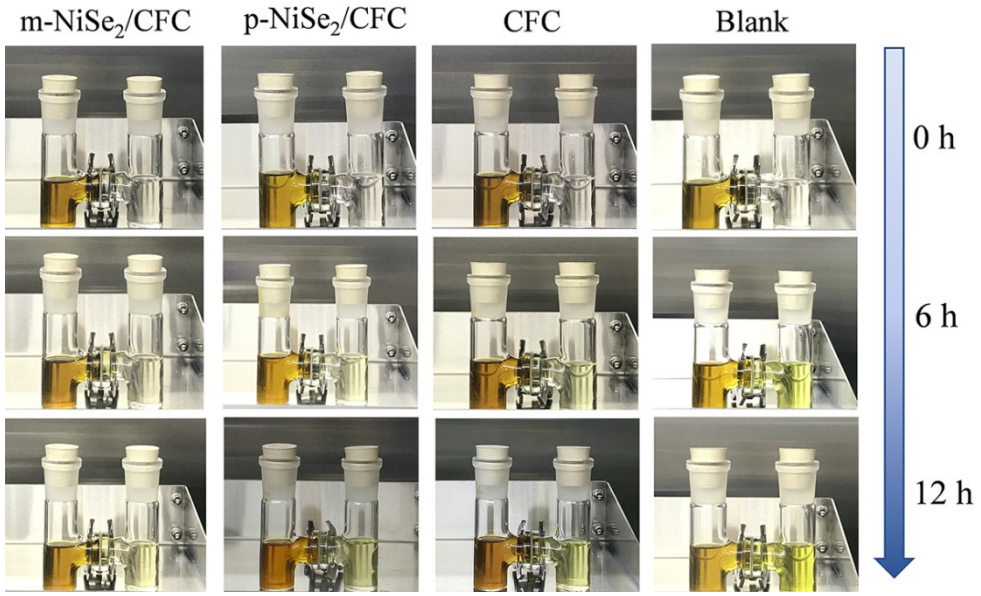

Fig. S3 Photographs of H-type glass cell filled with the lithium polysulfide (Li_2S_6) in DOL/DME solution (the left chamber) and the bare DOL/DME solvent (the right chamber), and separated by the bare Celgard separator (i.e., blank), the separator with a CFC film (i.e., CFC), the separator with a m-$NiSe_2$/CFC film (i.e., m-$NiSe_2$/CFC), and the separator with a p-$NiSe_2$/CFC film (i.e., p-$NiSe_2$/CFC) taken after testing durations of 0, 6, and 12 h.

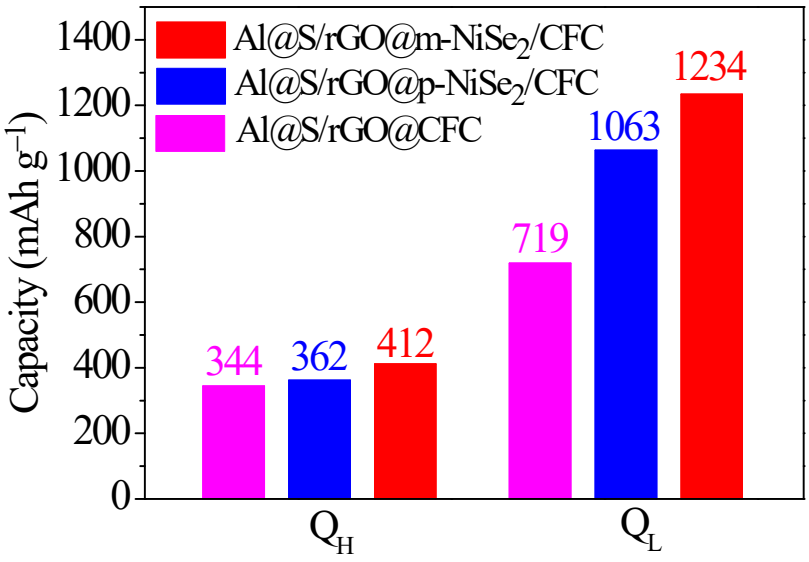

Fig. S4 The histogram of The Q_H and Q_L values of the Al@S/rGO@m-$NiSe_2$/CFC, Al@S/rGO@p-$NiSe_2$/CFC and Al@S/rGO@CFC cells at 0.2C rate.

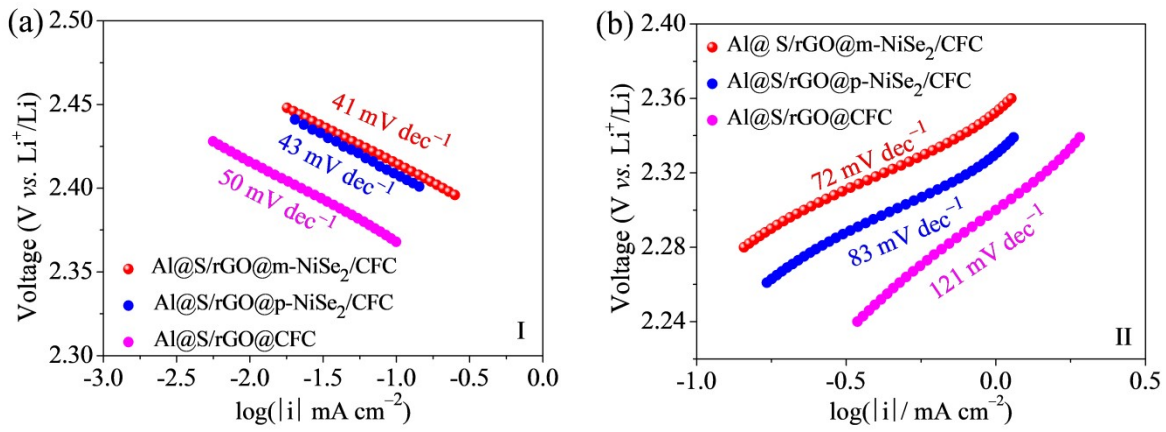

Fig. S5 Cathodic and anodic Tafel plots of the three cells obtained from the CV curves in Fig. 4e.

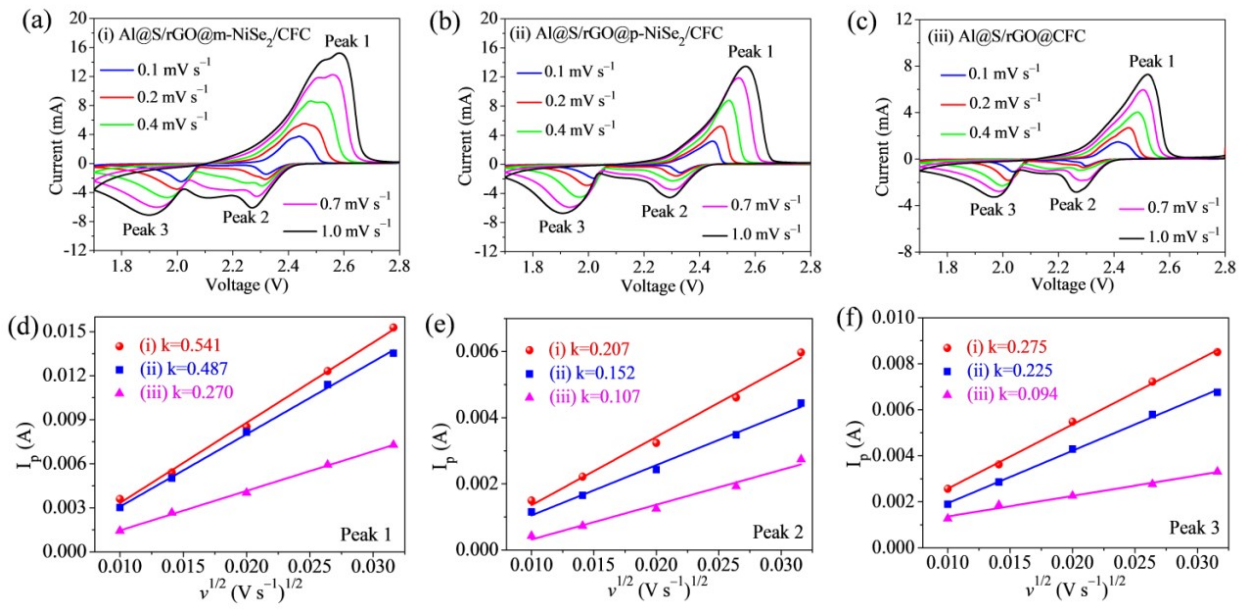

Fig. S6 (a-c) CV curves of (a) Al@S/rGO@m-$NiSe_2$/CFC, (b) Al@S/rGO@p-$NiSe_2$/CFC, (c) Al@S/rGO@CFC cells at various scanning rates. (d-f) The relationship between peak current (I_p) and square root of sweep rate ($v^{1/2}$) of the three cells.

Fig. S6a-c displays CV curves of the Al@S/rGO@m-$NiSe_2$/CFC, Al@S/rGO@p-$NiSe_2$/CFC and Al@S/rGO@CFC cells scanned at different rates of 0.1-1.0 mV s^{-1} to investigate the diffusion coefficients of Li-ions (D_{Li}). Each curve has one oxidation peak (peak 1) and two reduction peaks (peak 2 and 3). It is clear that the peak current (I_p) increases with increasing sweep rate (v). **Fig. S6d-f** shows the linear relationship between I_p and the square root of the sweep rate ($v^{1/2}$) of the three cells. The slopes (k) of peak 1, peak 2 and peak 3 for the Al@S/rGO@m-$NiSe_2$/CFC cell are estimated to be k_1=0.541, k_2=0.207 and k_3=0.275, respectively, which are much higher than those of the Al@S/rGO@p-$NiSe_2$/CFC cell (k_1=0.487, k_2=0.152 and k_3=0.225) and the Al@S/rGO@CFC cell (k_1=0.270, k_2=0.107 and k_3=0.094). The D_{Li} value can be calculated from the slopes of the linear fitting plots, according to the Randles-Sevcik equation:

$I_p = 2.686\times10^5 \cdot A \cdot n^{3/2} \cdot D_{Li}^{1/2} \cdot C_{Li} \cdot v^{1/2}$ (S1)

where I_p is the slope of the peak current, A is the area of electrode (A=1.13 cm^2), n is the number of electrons in the reaction (n=2), D_{Li} is the diffusion coefficient of Li-ions, v is the sweep rate, C_{Li} is the Li^+-ion concentration (C_{Li}=0.001116 mol cm^{-3}). Therefore, the D_{Li} values of Al@S/rGO@m-$NiSe_2$/CFC cell are calculated to be 31.79×10^{-8} cm^2 s^{-1} for peak 1, 4.65×10^{-8} cm^2 s^{-1} for peak 2, and 8.22×10^{-8} cm^2 s^{-1} for peak 3. These values are higher than those of the Al@S/rGO@p-$NiSe_2$/CFC cell (25.76×10^{-8} cm^2 s^{-1} for peak 1, 2.51×10^{-8} cm^2 s^{-1} for peak 2, and 5.50×10^{-8} cm^2 s^{-1} for peak 3). The Al@S/rGO@CFC cell has the lowest D_{Li} values (7.92×10^{-8} cm^2 s^{-1} for peak 1, 1.24×10^{-8} cm^2 s^{-1} for peak 2, and 0.96×10^{-8} cm^2 s^{-1} for peak 3).

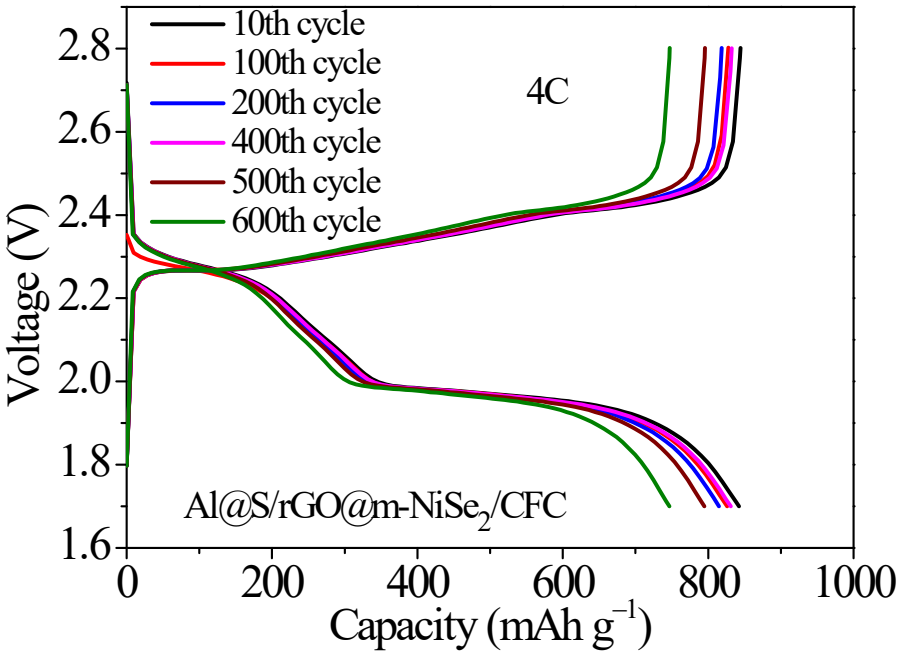

Fig. R7 Discharge/charge curves of the Al@S/rGO@m-$NiSe_2$/CFC cell at 4C rate for various cycles.

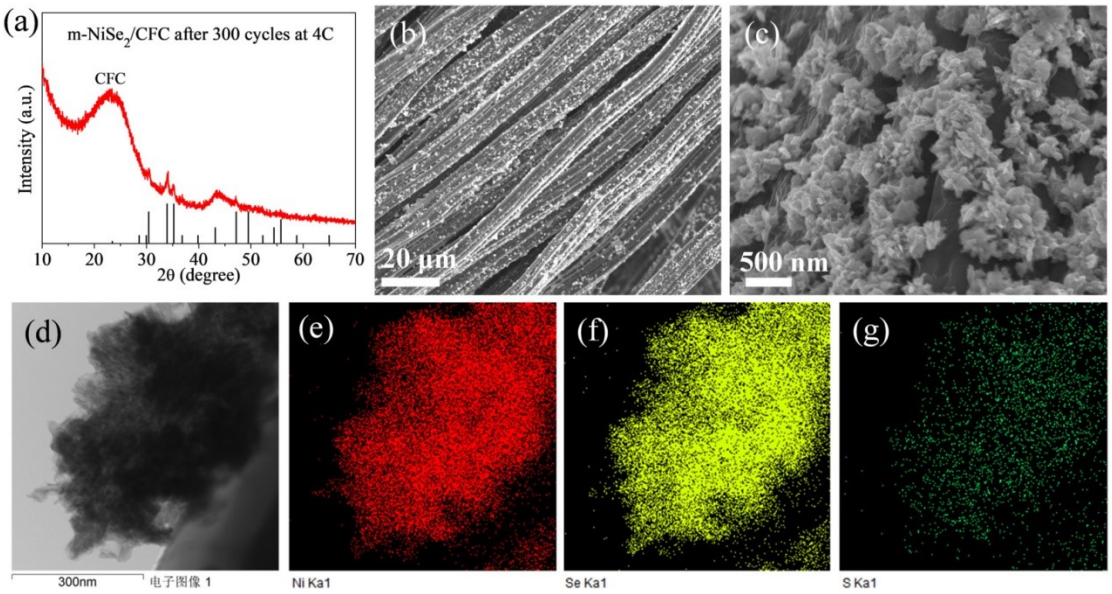

Fig. R8 (a) XRD pattern, (b,c) SEM images, (d-g) TEM image and corresponding EDX mappings of m-$NiSe_2$/CFC after 300 cycles at 4C.

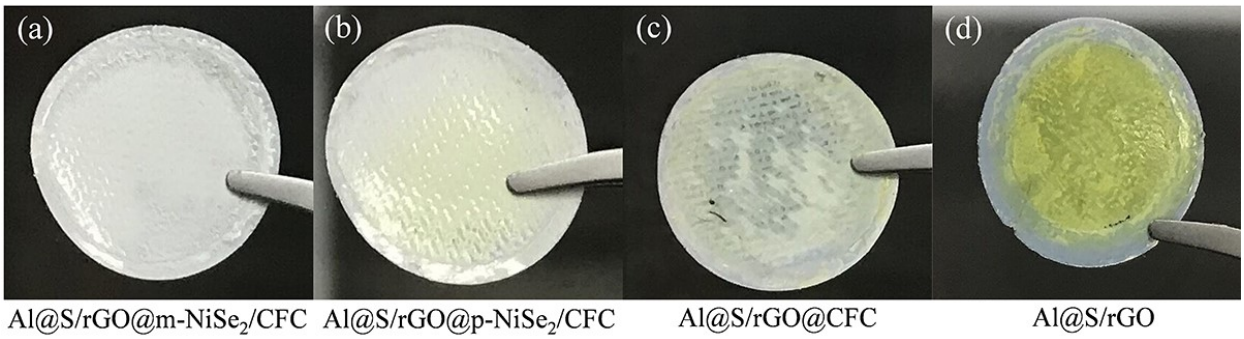

Fig. S9 Photographs of the separators obtained by disassembling the various cells after cycling at 1C rate for 100 cycles. Little color change is observed for the separator in the Al@S/rGO/m-$NiSe_2$/CFC cell, which indicates the m-$NiSe_2$/CFC film has a superior physiochemical blocking towards polysulfide migration.

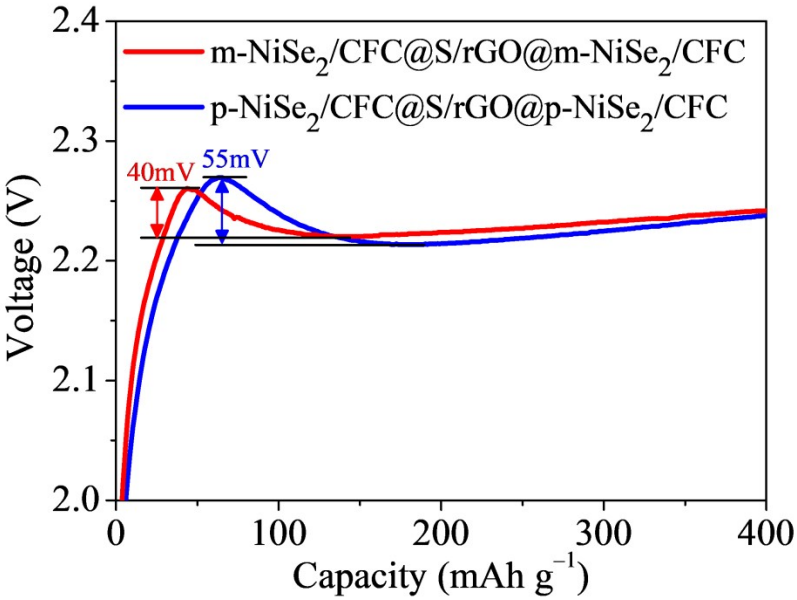

Fig. S10 The galvanostatic charge curves of m-$NiSe_2$/CFC@S/rGO@m-$NiSe_2$/CFC and p-$NiSe_2$/CFC@S/rGO@p-$NiSe_2$/CFC cells, showing the different charge barriers.

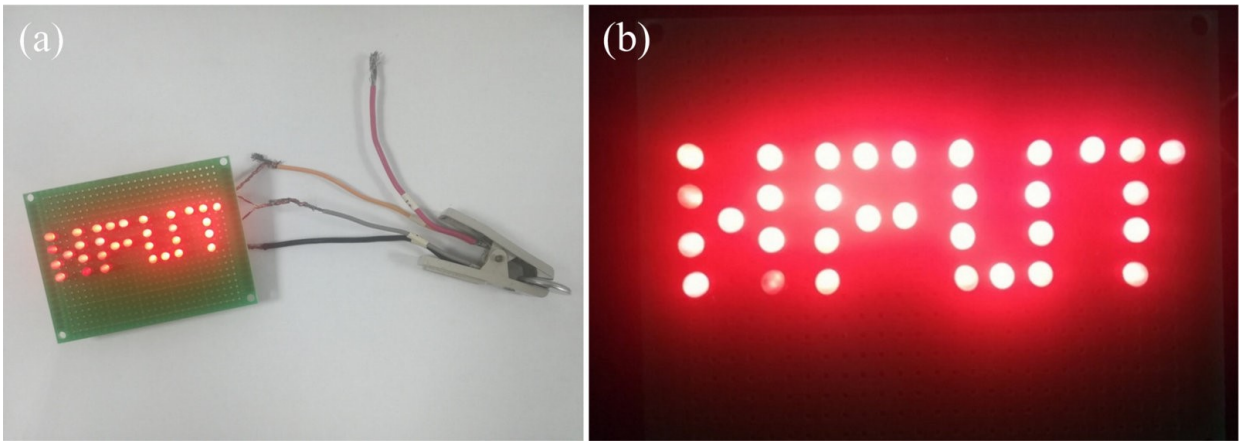

Fig. S11 Photograph of 32 LED lamps lighted by the m-$NiSe_2$/CFC@S/rGO@m-$NiSe_2$/CFC cell with a sulfur loading density of 2.5 mg cm^{-2}.

Table S2 Recent advances of nickel chalcogenide-based LSBs.

Current Collector	Cathode	Interlayer/ Separator	Sulfur Loading (mg cm^{-2})	Cycle Number/ Maintained Capacity (mAh g^{-1}) / Rate	Decay Per Cycle (%)	References
Al	S/rGO	m-$NiSe_2$/CFC	1.1	600/712/4C	0.028	Our work
		p-$NiSe_2$/CFC	1.1	600/508/4C	0.058	
m-$NiSe_2$/CFC	S/rGO	m-$NiSe_2$/CFC	2.5	100/1049/1C		
			4.5	100/829/1C		
$NiSe_2$/CC	S		5.0	2000/620/5C	0.019	J. Mater. Chem. A, 2019, 7, 15302-15308.
			12.0	100/830/0.1C		
Fe-$NiSe_2$/ACC	S		3.8	200/1018/0.1C	0.057	ChemSusChem, 2021, 14, 1710-1719.
			7.6	200/837/0.1C	0.083	
			9.9	200/923/0.1C	0.011	
Al	Co-$NiSe_2$@NC/ S		1.0	200/544.6/0.5C	0.043	Energy Technol., 2020, 8, 2000302.
Al	S/CNTs	$NiSe_2$	4.4	100/909/0.2C		ACS Appl. Energy Mater., 2021, 4, 3431-3438.
			8.8	100/886/0.2C		
Al	S@a-NiS_2		1.0	1200/954/1.5C	0.019	J. Mater. Chem. A, 2016, 4, 13395-13399
Al	S/NiS_2-C		1-1.2	200/730/0.5C		Nanoscale, 2016, 8, 17616-17622
Al	NiS_2/S/rGO			800/400/1C		J. Alloys Compd., 2018, 6, 804-812.
Al	3DC-CNTs-NiS_2/S		1.5	1000/600/1C	0.043	ACS Appl. Mater. Interfaces, 2020, 12, 17528-17537.
			6.5	50/738.5/0.5C		
Al	NiS_2-RGO /S/CNTs		5.0	400/715/0.5C	0.073	Adv. Energy Mater., 2018,
			7.0	100/757/0.2C		

			10.0	100/626/0.2C		8, 1801014.
			21.0	50/610/0.2C		
Al	S/CNTs	NiS_2@rGO/CNTs-Li	1.2	400/715/0.5C	0.073	ChemNanoMat, 2020, 6, 976-983.
Al	uNiS_2-ZnS/MMC-S		1.0	400/710.5/1C	0.033	Nanoscale, 2020, 12, 16201-16207.
			4.0	100/896.2/0.2C	0.116	
Al	NiS_2@NG-S		1.0	200/652/1C	0.13	ACS Appl. Energy Mater., 2020, 3, 3541-3552.